IBRACON Structures and Materials Journal
Revista IBRACON de Estruturas e Materiais
ISSN 1983-4195 ismj.org

ORIGINAL ARTICLE

Experimental performance of CA-50 steel shear connectors for composite structures in steel profiles and reinforced concrete

Desempenho experimental de conectores de cisalhamento de aço CA-50 para estruturas mistas em perfis de aço e concreto armado

Vanessa Carolaine de Sousa[a]
Arthur dos Reis Lemos Fontana[b]
Aarão Ferreira Lima Neto[a]

[a]Universidade Federal do Pará – UFPA, Núcleo de Desenvolvimento Amazônico em Engenharia, Programa de Pós Graduação em Engenharia de Infraestrutura e Desenvolvimeto Energético, Tucuruí, PA, Brasil
[b]Universidade Federal do Pará – UFPA, Programa de Pós Graduação em Engenharia de Recursos Naturais da Amazônia, Belém, PA, Brasil

Received 04 January 2024
Revised 25 April 2024
Accepted 14 June 2024

Abstract: Shear connectors are essential elements in composite structures of steel and concrete as they ensure the interaction between materials and the transfer of forces. In this research, seven models of shear connectors made from bent CA-50 steel bars were tested. The models varied in bar diameter, reinforcement ratio, and inclination relative to the metal profile's flange. The results showed that the connector with a 12.5 mm diameter (model A1) exhibited the best performance in terms of strength and ductility. Connectors with a 10.0 mm diameter (models B1 and B2) also showed satisfactory results. The inclination of the connectors did not significantly influence the strength of the models. However, a higher tendency for uplift strain was exhibited in the inclined connectors.

Keywords: composite beams, composite structures, shear connector, push-out test.

Resumo: Conectores de cisalhamento são elementos essenciais nas estruturas mistas de aço e concreto, pois garantem a interação entre os materiais e a transferência de esforços. Nesta pesquisa, foram ensaiados 7 modelos de conectores de cisalhamento confeccionados com vergalhões de aço CA-50 dobrados. Os modelos variaram em bitola das barras, taxa de armadura e inclinação em relação à mesa do perfil metálico. Os resultados mostraram que o conector com bitola de 12,5 mm (modelo A1) obteve o melhor desempenho em termos de resistência e ductilidade. Os conectores com bitola de 10,0 mm (modelos B1 e B2) também apresentaram resultados satisfatórios. A inclinação dos conectores não apresentou influência significativa na resistência dos modelos. No entanto, os conectores inclinados apresentaram maior tendência à deformação por *uplift*.

Palavras-chave: vigas mistas, estruturas mistas, conector de cisalhamento, push-out test.

How to cite: V. C. Sousa, A. R. L. Fontana, and A. F. L. Lima Neto, "Experimental performance of CA-50 steel shear connectors for composite structures in steel profiles and reinforced concrete," *Rev. IBRACON Estrut. Mater.*, vol. 17, no. 3, e17315, 2024, https://doi.org/10.1590/S1983-41952024000300015

1 INTRODUCTION

The use of composite structures with steel profiles and reinforced concrete has been occurring since the early 1920s, experiencing growth since then, with widespread application in bridges in the 1950s and in buildings around the 1960s [1]. This approach offers the possibility of more slender sections, faster execution, and the potential for reduced framing, as each material is subjected to the forces it supports more efficiently: steel to tension and concrete to compression. The concrete slab also assists the steel beam against torsion and buckling, providing greater stiffness.

Corresponding author: Aarão Ferreira Lima Neto. E-mail: aaraol@yahoo.com.br
Financial support: None.
Conflict of interest: Nothing to declare.
Data Availability: The data that support the findings of this study are openly available on the PPGINDE/UFPA website at https://drive.google.com/file/d/1P6wZ-Lsm2iCWMh7suiYmT1ODilx6pzqb/view?pli=1.

Composite beams offer several advantages over conventional reinforced concrete beams, such as section reduction to resist the same loads (utilizing the characteristics of steel and reinforced concrete), the possible lack of formwork and framing, and a reduction in the self-weight and volume of the structure. In comparison to steel structures, it enables greater structural stiffness and a considerable reduction in the consumption of reinforcement [2].

For an effective use of the properties of the composite beams, it is necessary to use connectors that determine the interaction level between the elements and facilitate the transfer of forces between the metal profile and the concrete slab. Therefore, the selection of the connector type and its correct design is essential.

Although shear connectors are fundamental in composite beams, the current codes [3-6] do not cover calculations and guidelines for their use. Even though Eurocode 4 [6] provides a test for evaluating the strength of connectors not covered by the codes, only stud and U-profile connectors are covered by current codes, including design parameters, limiting the use of other connector types that could be more effective to specific design scenarios.

In this context, the development and study of connectors that bring construction ease, coupled with available materials at a lower cost, compared to more traditional options like studs, are crucial.

The connectors in this research (bent CA-50 steel bars) are simply designed and made from materials easily found on the market, offering a more affordable alternative when compared to steel plates and studs, commonly used in composite structures. As continuous connectors, they exhibit higher assembly productivity and do not require specific equipment for installation, making them easily executable in various design situations.

Furthermore, the tested connectors serve as a viable alternative to stud connectors, which come with some disadvantages in terms of construction (in addition to their high cost), as they require both specialized equipment and workforce for assembly, typically found only in major urban centers. In less technologically developed states and in the countryside, the assembly technology for stud connectors is not readily available, either making their use impractical or significantly increasing the cost of hiring services from other locations.

The objective of this study is to experimentally analyze, through direct shear tests known as push-out tests, the performance of shear connectors made of bent CA-50 steel bars, using different diameters and varying the positioning, for the application in composite structures of steel profiles and reinforced concrete elements.

2 MATERIALS AND EXPERIMENTAL PROGRAM

The experimental program consists of 7 specimens subjected to push-out tests, following the recommendations of Eurocode [6]. The specimens were made for push-out tests and performance evaluation in accordance with the criteria established by the code. Each specimen consisted of 1 steel element in an I-profile and 2 reinforced concrete slabs connected by the shear connectors designed for this research. The connectors were made from CA-50 steel bars, bent at 90° angles, forming a connector with multiple legs. The variables among the models include connector diameter, number of legs, and the final geometry of the connector. Table 1 presents the characteristics of the tested models.

Table 1. Characteristics of push-out tested models

Specimen	Shear connector					
	Type of connector	Diameter (mm)	No. of legs	Length of I-Profile (mm)	No. of connectors	Total steel area (mm^2)
A1	Straight	12.5	4	800	4	1963.50
A2	Inclined					
B1	Straight	10.0	6			1884.96
B2	Inclined					
C1	Straight	8.0	6			1206.37
C2	Straight	8.0	6		6	1809.56
D	Module	6.3	32		2	1995.04
Reinforced concrete slab:						
Concrete compressive strength (f_{ck}) = 25 MPa; Thickness = 150 mm.						

The connectors studied in this research are variations of those tested by Souza [7], which showed good potential for use, presenting good strength and ductility results in relation to the failure mode during the conducted tests. Model A1 has, for each slab, two connectors with 4 legs, made of CA-50 steel with a diameter of 12.5 mm, positioned as shown in Figure 1.

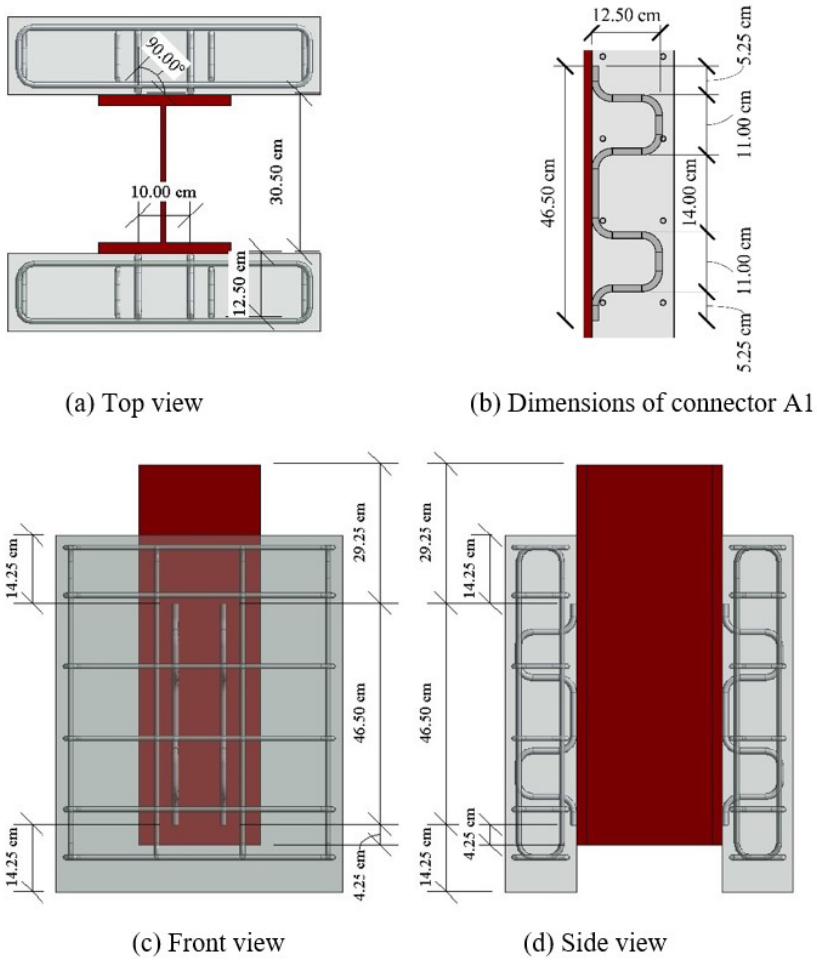

(a) Top view (b) Dimensions of connector A1

(c) Front view (d) Side view

Figure 1. Dimensions of the specimen and connector A1

Model A2 also features two connectors with 4 legs, made of CA-50 steel with a diameter of 12.5 mm, but with the connectors inclined at approximately 68º, as shown in Figure 2.

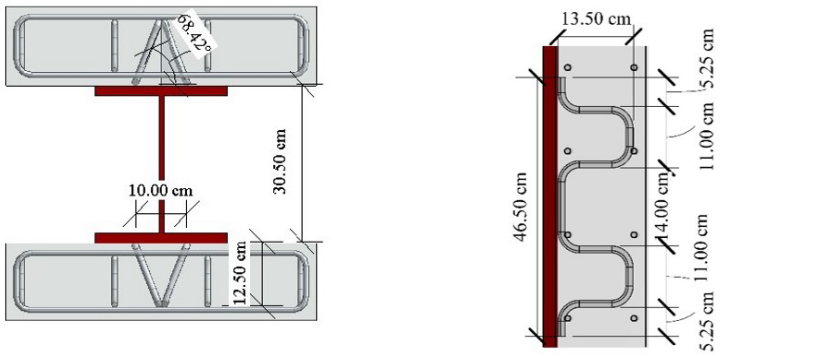

(a) Top view (b) Dimensions of connector A2

Figure 2. Dimensions of connector A2

Model B1, like model A1, is a module formed by two connectors joined by welded bars and positioned at 90º to the surface of the metal profile. The connectors have 6 legs and were made with CA-50 steel with a diameter of 10.0 mm (Figure 3).

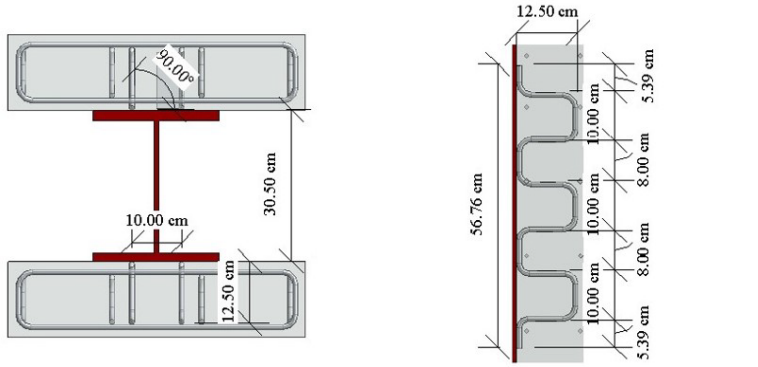

(a) Top view (b) Dimensions of connector B1

Figure 3. Dimensions of connector B1

Model B2 also features two connectors with 6 legs on each slab, made of CA-50 steel with a diameter of 10.0 mm, but with the connectors inclined at approximately 68º, as shown in Figure 4.

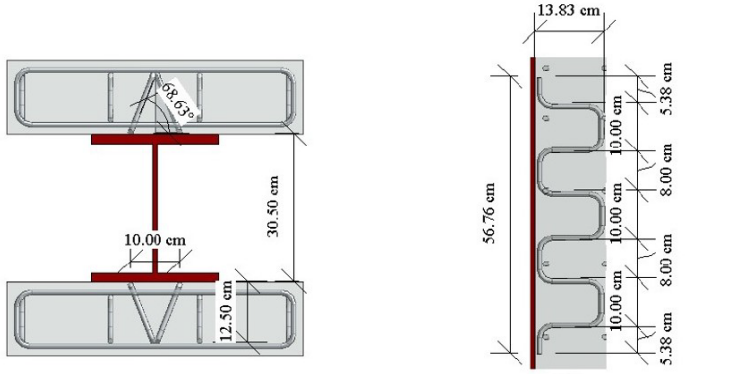

(a) Top view (b) Dimensions of connector B2

Figure 4. Dimensions of connector B2

Experimental model C1 has, in each of its slabs, a pair of connectors made of CA-50 steel with a diameter of 8.0 mm and 6 legs each, as shown in Figure 5.

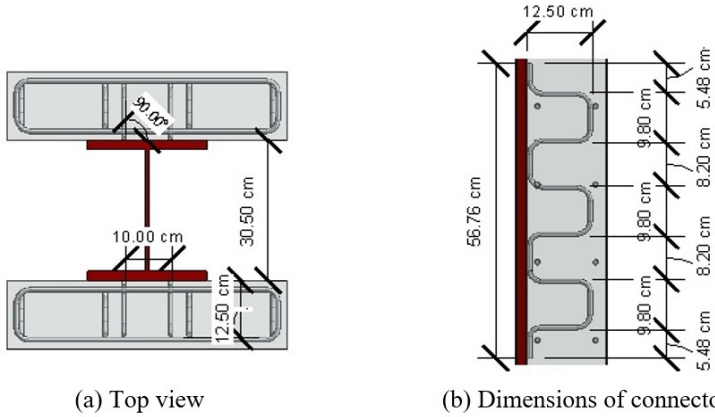

(a) Top view (b) Dimensions of connector C1

Figure 5. Dimensions of connector C1

Experimental model C2 has, in each of its slabs, three connectors made of CA-50 steel with a diameter of 8.0 mm and 6 legs each, as shown in Figure 6.

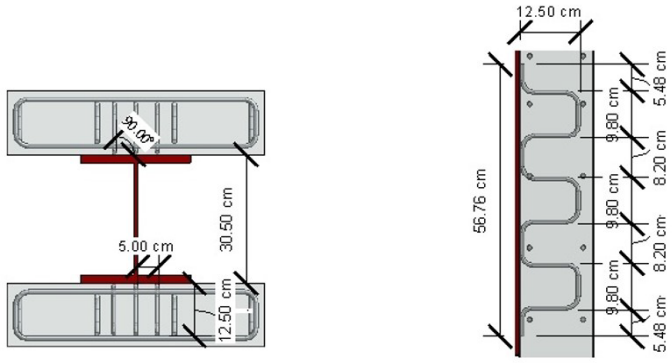

(a) Top view (b) Dimensions of connector C2

Figure 6. Dimensions of connector C2

Experimental model D is a module composed of 32 legs, made of steel with a diameter of 6.3 mm, with small steel bars with a diameter of 5.0 mm welded at the top to assist in the construction of the module. Figure 7 shows the details of connector D.

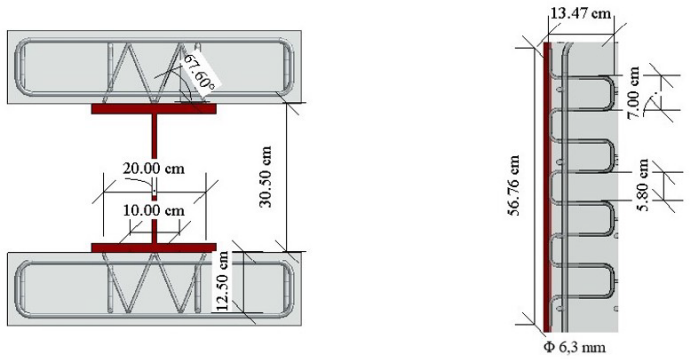

(a) Top view (b) Dimensions of connector D

Figure 7. Dimensions of connector D.

2.1 Material Characterization

2.1.1 Concrete

Following the recommendations of ABNT NBR 5738 [8], cylindrical specimens with a diameter of 100 mm and height of 200 mm were molded. These specimens were used in the characterization tests of the concrete regarding compressive strength, diametral compression strength, and modulus of elasticity, following the guidelines of codes [9], [10], and [11]. In the fresh state, the slump test was carried out, following the recommendations of NBR NM 67 [12].

The concrete mix used is 1: 2.3: 2.5: 0.44 (cement: sand: gravel: w/c ratio), with known properties and used by Freitas [13]. The concrete exhibited a slump of 4 ± 1 cm. Table 2 contains the results of all concrete tests.

Table 2. Mechanical Properties of Concrete

CP	f_c (MPa)	f_{ct} (MPa)	E_c (GPa)
1	26.24	2.71	28.55
2	22.83	2.51	27.43
3	28.22	2.78	29.10
4	22.80	2.44	27.43
Average	25.02	2.61	27.99
Standard Deviation	2.68	0.16	0.83

2.1.2 Steel of Slabs and Connectors

The mechanical properties of the steel used in slabs and shear connectors were determined following the recommendations of ABNT NBR 6892 [14]. The yield stress and ultimate stress were obtained for each steel diameter, and the average values are presented in Table 3.

Table 3. Properties of the steel used in slabs and connectors

Ø	f_{ys} (MPa)	f_u (MPa)	$\mathcal{E}_{ys}$ (‰)
6.3	637.53	677.83	2.92
8.0	549.50	582.46	2.51
10.0	674.28	712.16	3.08
12.5	591.38	614.85	2.84

2.1.3 Steel of I-profile and weld

The main characteristics of the I-profile steel were determined through metallography in a sample taken from the profile and tensile tests on 3 standardized samples according to ASTM-E8 [15]. The weld that joins the connectors to the I-profile was carried out in the Mechanical Engineering Laboratory of CAMTUC – UFPA, with E7018 electrodes, with a diameter of 3.25 mm along the entire surface of the connector with the profile's flange, on both sides of the legs, ensuring that the failure did not occur at the connection.

Samples from the metallographic test were analyzed through an optical microscope; Figure 8 shows a 200x magnification obtained in the microscopic analysis. And in Table 4 presents the areas of ferrite and pearlite in the samples taken from the I-profile.

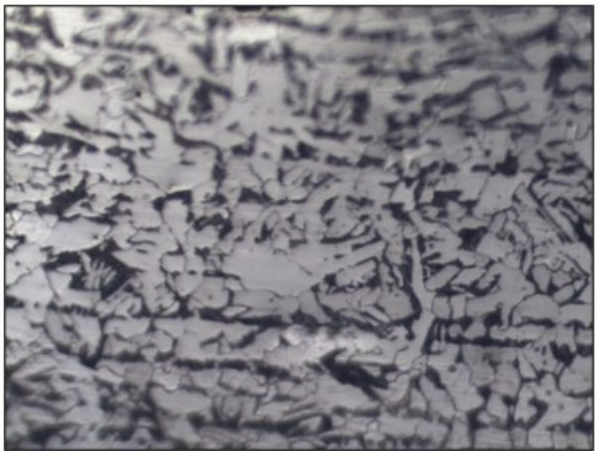

Figure 8. Microstructural characterization of the steel in the profile, 200x zoom

Table 4. Average grain area in the profile's sample.

Average area of pro-eutectoid ferrite and pearlite grains.		
	Pro-eutectoid Ferrite	Pearlite
Area $(\mu m)^2$	63.987	36.013

Knowing the content of free ferrite, the carbon content in the steel can be calculated using the Equation 1:

$$\%_{\propto L} = \left(1 - \frac{C_o}{0.77}\right) * 100 \quad (1)$$

Where,

$\%_{\propto L}$ is the percentage of free ferrite;

C_o. is the percentage of carbon in the steel.

Through the calculations, a carbon content of 0.2773% was obtained. Steels with concentrations between 0.25 and 0.60% are considered medium-carbon steels. The classifications and specifications of steel are made by the Society of Automotive Engineers (SAE) and the American Iron and Steel Institute (AISE), designating it as a 1028 steel, as shown in Table 5 [16].

Table 5. SAE/AISI Classification of the steel in the profile

Carbon Content	Classification
0,2773%	SAE/AISI 1028

For the tensile tests, 3 specimens were tested following pre-established code criteria. Figure 9 shows the Stress x Strain curves for the three specimens tested for tensile strength, and the properties obtained in the test are presented in Table 6.

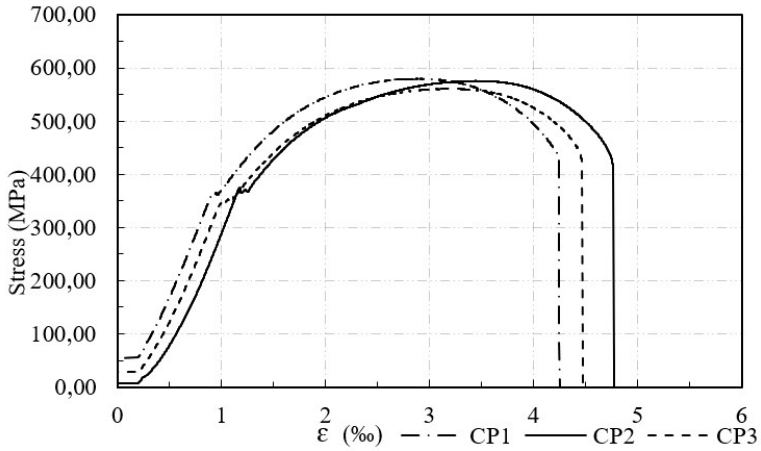

Figure 9. Stress x Strain curves of the specimens tested for tensile strength

Table 6. Mechanical properties of the I-profile steel

Sample	f_{ysI} (MPa)	f_{usI} (MPa)	$\varepsilon_{máx}$ (‰)	E_{sI} (GPa)
1	364.29	579.71	4.27	443.16
2	375.17	575.62	4.80	433.81
3	345.34	560.64	4.49	439.18
Average	361.60	571.99	4.52	438.72
Standard Deviation	15.10	10.04	0.27	4.70

2.1 Specimen Instrumentation

To measure the strains of the steel connectors and the slab reinforcement, strain gauges were used, with temperature self-compensation and copper wires welded to the terminals. The gauges were positioned 3.5 cm away from the flange of the profile to avoid influences from the bend of the connector leg for the strain measurement. Additionally, the strain gauges were applied only after the welding, to prevent the risk of damaging them.

One of the bars of the slab reinforcement was also monitored, as shown in Figure 10. The selection of the bar was based on the results from Barbosa [17].

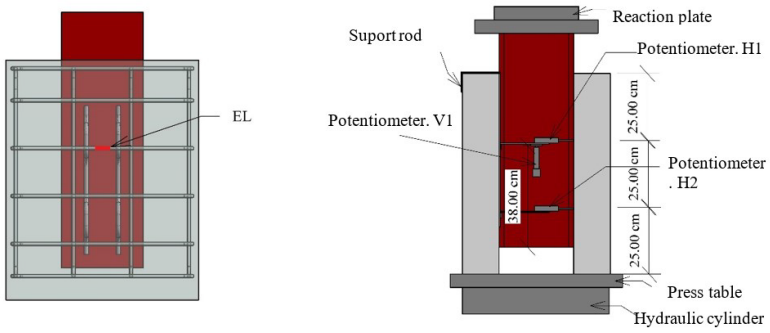

a) Instrumentation of the slab steel b) Testing system

Figure 10. General instrumentation of the models

2.2 Concrete casting and push-out test

The casting of the models was carried out at the Civil Engineering Laboratory of UFPA (Tucuruí Campus) using concrete with f_{ck} of 25 MPa and a slump value of 4 ± 1 cm. Both the push-out models and the cylindrical specimens were cast on the same day. The concrete poured onto the slabs was vibrated with the aid of an electric concrete vibrator.

The push-out tests followed the recommendations of Eurocode 4 [6]. Throughout the test, there were measurements of: the vertical displacement of the profile in relation to the slabs; the transverse displacement of the slabs; the strain data of the slabs and the connectors steel; and the strain of the slab concrete.

The machine used for the tests is a hydraulic press from WOLPERT, model 300-D-74, with a maximum loading capacity of 300 tons, monitored by the commercial software Tesc, owned by the Civil Engineering Laboratory of UFPA-CAMTUC. The monitoring devices were connected to the data acquisition module ADS 2000, from *Lynx Tecnologia*. Figure 11 shows one of the specimens properly positioned for the test.

Figure 11. Model A2 positioned for the test.

3 RESULTS AND DISCUSSION

3.1 Failure Loads and Design Strength

The estimates of failure loads were obtained through computer simulation using the commercial software Ansys, through a model calibrated with data obtained by Souza [7] and the results obtained from material tests. The figure illustrates the results obtained from both simulations and experimental tests (Figure 12).

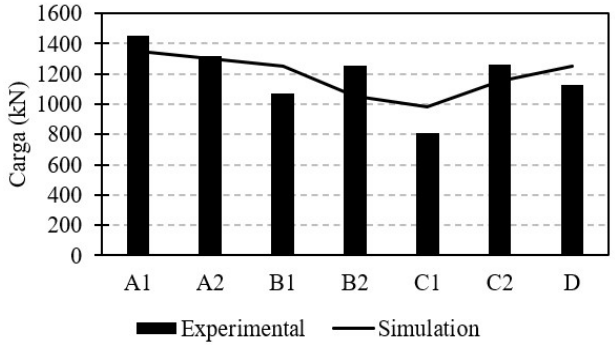

Figure 12. Experimental loads and from the computer simulation in Ansys

During the tests, the loading rate was kept so that failure did not occur in less than 15 minutes after the completion of the loading and unloading cycles, as recommended by Eurocode 4 [6]. Table 7 presents the results of the maximum load reached in the tests, the characteristic strength, and the design strength for the analyzed models.

Table 7. Maximum load reached in each model

Model	No. of connectors	A_{st} (cm^2)	P_{max} (kN)	P_{rk} (kN)	P_{rd} (kN)	P_{max}/A_{st} (kN/cm^2)
A1	4	19.64	1453.40	327.02	221.19	74.02
A2			1318.90	296.75	200.72	67.17
B1		18.85	1068.36	240.38	159.72	56.68
B2			1254.16	282.19	187.50	66.54
C1		12.06	808.47	181.91	115.50	67.02
C2	6	18.10	1262.46	189.37	120.23	69.77
D	2	19.95	1126.80	507.06	293.95	56.48

P_{max}: Maximum load of the model. P_{rk}: Characteristic strength per connector. P_{rd}: Design strength per connector. A_{st}: Total steel area.

The A1 model proves to be more resistant than the A2 model by approximately 10%. Comparing the results of this research with those obtained by Souza [7], who tested the RT-type connector, equivalent to the A1 connector, it is seen that the model in this study surpassed the maximum load supported by the RT connector by about 12%. Based on the results presented in Table 7, Figure 13a shows the failure load by model, and Figure 13b the maximum load/steel area ratio of the connector for all tested models.

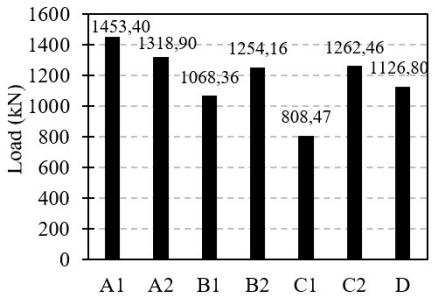

(a) Failure load by model

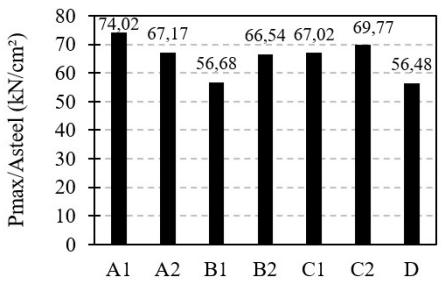

(b) Maximum load x steel area ratio of the connector cross-section

Figure 13 – Model strength results

As seen in Figure 13b, connectors A1 and C2 exhibit the best performance when relating maximum loads to the steel areas of the connector cross-sections. Models B1 and D present the lowest values.

Model A1 excels in terms of the maximum load achieved in the test and also demonstrates the best utilization of the cross-sectional area, achieving 74.02 kN/cm^2, surpassing the other connectors in this study, representing a gain of 11.32%

when compared to the average. Additionally, it outperforms connectors studied by Barbosa [17] and Souza [7], whose best-performing connectors achieved 68.83 kN/cm^2 and 64.38 kN/cm^2, gains of 10.75% and 11.50%, respectively.

On the other hand, models B1 and D exhibited the poorest performance in Maximum load x Steel area, being about 9% below the average of all models in this study, with values of 56.68 kN/cm^2 and 56.48 kN/cm^2, respectively, while the average value of all researched connectors exceeds 65 kN/cm^2.

3.2 Relative displacement between the I-profile and the concrete slabs

Figure 14 shows the Load x Sliding behavior of all tested models.

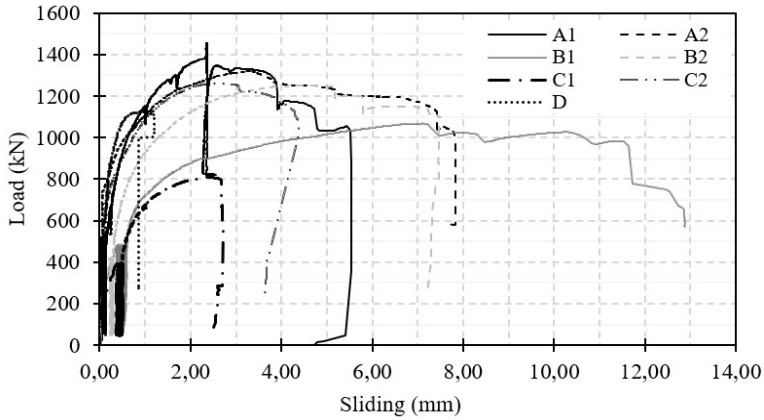

Figure 14 - Longitudinal sliding of the models

Until the end of the cyclic loading phase, most tested models remained with about no relative sliding, except for B1 and C1, which showed approximately 0.60 mm and B2 with 0.30 mm of sliding.

The smallest sliding values achieved at maximum loading were from models C1 and D. Both failed abruptly shortly after reaching the peak load, preventing the acquisition of sliding data in the post-peak phase. Model D proves to be the stiffest among those analyzed, failing with approximately 1.20 mm of longitudinal sliding between the slabs and the metal profile.

On the other hand, the other models exhibited greater ductility for the same level of loading, with a satisfactory record of the load drop phase after reaching the maximum load. Models A2, B1, and B2 were the most ductile among those analyzed.

Figure 14 shows that Model B1 behaves differently from the others, reaching over 7.0 mm of sliding at maximum loading, with some small drops and load recoveries until close to the 11.60 mm sliding when it experiences a considerable drop in loading.

Analyzing the Force x Sliding graphs for each model, the values of P_k, which is the characteristic strength corresponding to $0.9P_{máx}$, δ_u, representing the sliding corresponding to $0.9P_{max}$, and δ_{uk}, which is the characteristic sliding capacity, were determined. These values are used in the classification of connectors regarding their ductility, according to the recommendations of Eurocode 4 [6].

The P_k value corresponds to 90% of the maximum load reached in the test ($0.9.P_{máx}$) after the peak, and corresponds to the sliding δ_u, which is used to find the value of the characteristic sliding capacity δ_{uk}, which corresponds to 90% of δ_u. Table 8 presents the results of maximum loads and the values of P_k, δ_u and δ_{uk} for the tested models, along with the classification according to Eurocode [6].

Among the connectors classified as rigid, Model D exhibited the greatest stiffness, with a characteristic sliding capacity of only 1.09 mm. The highest ductility was observed in Model B1, which had a δ_{uk} of 10.47 mm. Classifying the connectors in ascending order of ductility leads to the following sequence: D, A1, C1, C2, A2, B2, and B1.

During the load incline phase, Models B1 and C1 show higher sliding than the others for the same levels of loading. Model B1 reaches a characteristic sliding of 10.47 mm (δ_{uk}), while Model C1 shows abrupt failure shortly after the peak load is reached, with a characteristic sliding (δ_{uk}) of 2.42 mm.

According to Eurocode 4 [6], flexible connectors can be considered to have ideal plastic behavior, exhibiting considerable plastic strains for service loads, which is a significant advantage in terms of safety. On the other hand, rigid connectors have the advantage of being less susceptible to material fatigue failure since they do not exhibit significant plastic strain for service loads.

Table 8. Results of longitudinal sliding for the analyzed models

Model	P_{max} (kN)	P_k (kN)	δ_u (mm)	δ_{uk} (mm)	Classification Eurocode 4 (2004)
A1	1453.40	1308.06	2.36	2.13	Rigid
A2	1318.90	1187.01	6.76	6.08	Ductile
B1	1068.36	961.52	11.63	10.47	Ductile
B2	1254.16	1128.75	7.23	6.50	Ductile
C1	808.47	727.61	2.69	2.42	Rigid
C2	1262.46	1136.22	4.24	3.82	Rigid
D	1126.80	1014.12	1.21	1.09	Rigid

P_{max}: Maximum load of the model. P_k: Characteristic strength, $0.9*P_{máx}$. δ_u: Sliding corresponding to P_k. δ_{uk}: Characteristic sliding capacity corresponding to $0.9*\delta_u$. (If $\delta_{uk} \geq 6.00$ mm, the connector is classified as ductile)

Overall, the connectors in this research proved to be more rigid than the models tested by Barbosa [17] and Souza [7]. The RT-type connectors tested by Souza [7], which are like the connectors A1 in this study, reached a characteristic sliding (δ_{uk}) of 18.9 mm, while Model A1 achieved only 2.13 mm of characteristic sliding. The models tested by Barbosa [17] can reach 25 mm of δ_{uk}, and even their least ductile model exceeds 8 mm of δ_{uk}.

3.3 Transverse Separation of the Slabs

The behavior regarding uplift at the two points analyzed by the two positioned potentiometers is similar. For analysis and classification criteria regarding the resistance to uplift of the studied connectors, the average of the values from the two potentiometers in each analyzed model was used. To evaluate the connector's performance concerning the uplift effect, the values of transverse separation of the slabs for a loading equal to 80% of the model's failure load (Up_{80}) and the sliding for the same loading (δ_{80}) were determined. The obtained uplift results are compiled in Table 9.

Table 9. Uplift recorded for the tested models

Model	P_{max} (kN)	P_{80} (kN)	Up_{80} (mm)	δ_{80} (mm)	Up_{80}/δ_{80}
A1	1453.40	1162.62	1.16	1.06	1.09
A2	1318.90	1055.12	1.09	0.80	1.36
B1	1068.36	854.69	0.82	1.79	0.46
B2	1254.16	1003.33	0.77	1.28	0.60
C1	808.47	646.77	0.33	0.91	0.36
C2	1262.46	1009.97	0.48	0.75	0.64
D	1126.80	901.44	0.50	0.27	1.85

P_{max} - Maximum load resisted by the experimental model. P_{med} - Average of the maximum loads of the experimental models. Up_{80} - Uplift values for $0.8P_{max}$. U_pP_{max} - U_{plift} for the maximum load resisted by the experimental models. δ_{80} - Sliding corresponding to $0.8P_{max}$.

The uplift values (Up_{80}) recorded by the connectors, in ascending order, were for the models: C1, C2, D, B2, B1, A2, and A1. According to Eurocode 4 [6], the ratio between Up_{80} and δ_{80} should be less than 50% for the connectors to exhibit satisfactory behavior regarding uplift. Thus, the only models that showed satisfactory performance in this aspect were the connectors B1 and C1. Although B1 had a high Up_{80} value, it managed to achieve the minimum performance due to the ductility of the model, which was the highest among the analyzed models.

Among the other connectors, models B2 and C2 showed the best performances with Up_{80}/δ_{80} ratios of 0.60 and 0.64, respectively. Model D was the negative highlight, with a Up_{80}/δ_{80} ratio of 1.85, presenting 0.50 mm of uplift compared to only 0.27 mm of longitudinal sliding at $0.8P_{máx}$.

Observing models A and B, an increase in the Up_{80}/δ_{80} ratio is noted for models A2 and B2 compared to models A1 and B1, respectively. The increases were 25% and 30%, respectively, so that the connectors inclined relative to the flange of the I-profile presented worse performance regarding uplift. A similar trend was also observed in the tests of Souza [7] where the TII and TRI connectors, positioned inclined to the flange, showed worse uplift performance compared to the TI and TR connectors, which are straight.

Figure 15 shows a bar graph that better highlights the performance of the connectors and the performance discrepancy among the analyzed models. In general, the B and C connectors showed the best performances, and although B2 and C2 did not reach the minimum performance stipulated by the code, they obtained results very close to the maximum of 50% for the Up_{80}/δ_{80} ratio.

It is noted that the diameters of 10.0 mm and 8.0 mm, for models B and C, respectively, achieved better results in the Up_{80}/δ_{80} ratio compared to the 12.5 mm ones (models A). Model D, with a smaller diameter, exhibits the poorest performance, which may have occurred due to the complex geometry of the connector, thereby increasing its stiffness.

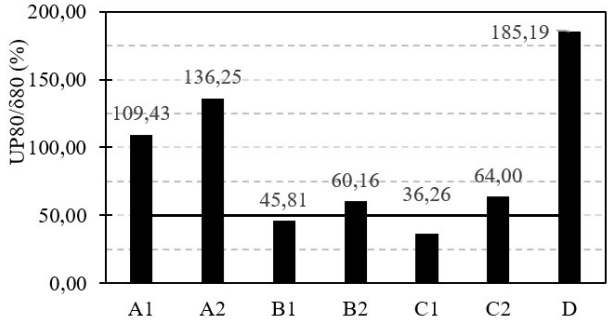

Figure 15. Up_{80}/δ_{80} ratio for all tested models

3.4 Strains of Shear Connectors and Slab Reinforcement

3.4.1 Strain of Shear Connectors

The strains of the shear connectors for each studied model are shown in the graphs in Figures 16 and 17.

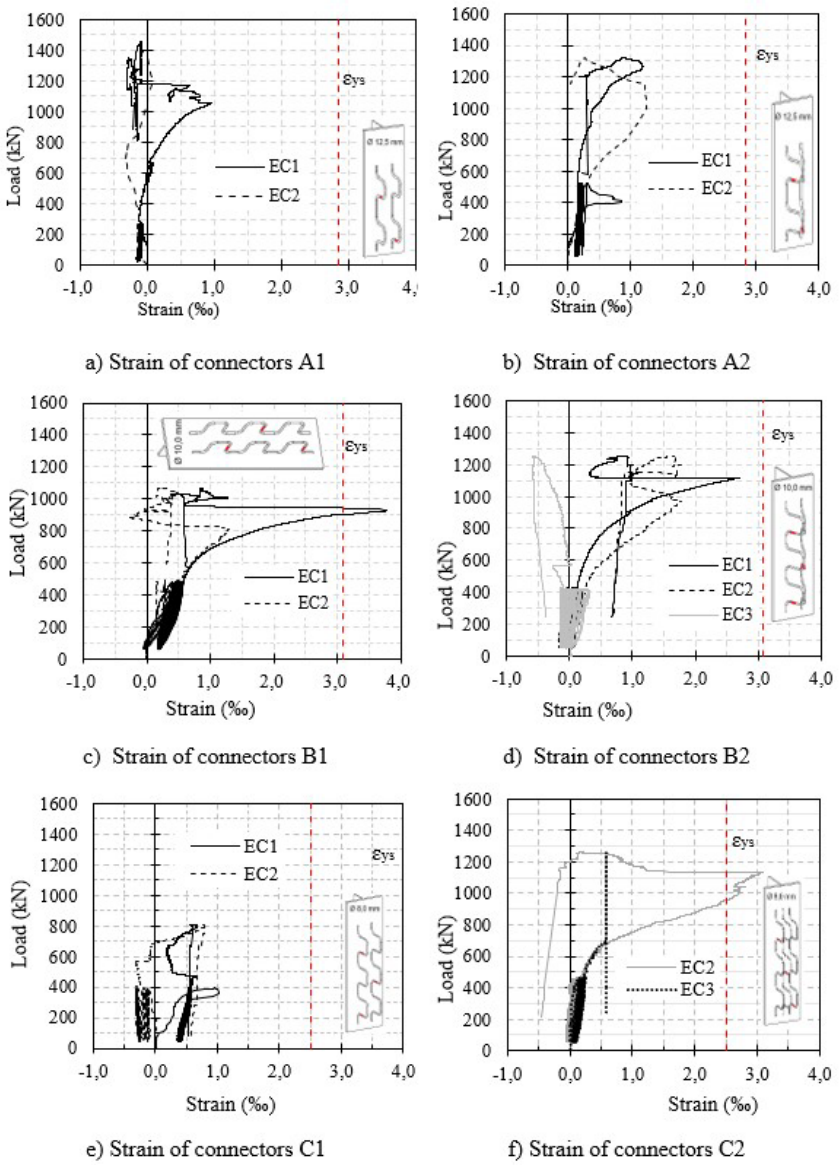

Figure 16. Strain of connectors

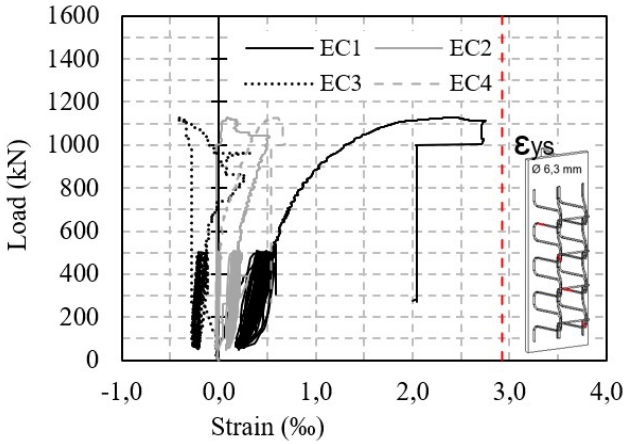

Figure 17. Strain of connectors D

In general, the connectors that exhibited the highest strain in the push-out test belonged to models B1, B2, C2, and D, reaching 3.78‰, 2.70‰, 3.09‰, and 2.75‰, respectively. Observing the graphs of models A1 and A2, respectively, it is evident that for the same loading levels, strains are higher in both connectors of model A2. For a load of 800 kN, connectors in model A1 show strains, in modulus, of 0.2‰ to 0.3‰, while connector EC2 in model A2 exhibits almost 1.0‰. Both connectors in A2 showed elongation up to near the 1200 kN load, after which strains gradually decreased until the end of the test (Figures 16a and 16b).

Models B1 and B2 exhibit similar strain curves in connectors EC1 and EC2 (Figures 16c and 16d). In general, there were gradual elongation strains up to a maximum point, followed by a sudden regression, and again elongation strains until the end of the test. In both models, the highest strain was observed in connector EC1, reaching strains of approximately 3.7‰ and 2.7‰ in models B1 and B2, respectively. After the 1150 kN load, connectors EC2 and EC3 in model B2 follow the same strain pattern, resuming elongation and deforming until the end of the test.

In model C1, connectors EC1 and EC2 exhibited strains of 0.6‰ and 0.8‰, respectively (Figure 16e). Analyzing the graph in Figure 16f for model C2, it is noted that EC2 reaches just over 3‰ elongation strain with a load slightly above 1100 kN, after which it starts to exhibit compression strains, with the increase in load reaching negative strain values after the model failure.

3.4.2 Slab Reinforcement

Figure 18 illustrates the Load x Specific Strain graph of the monitored slab bars.

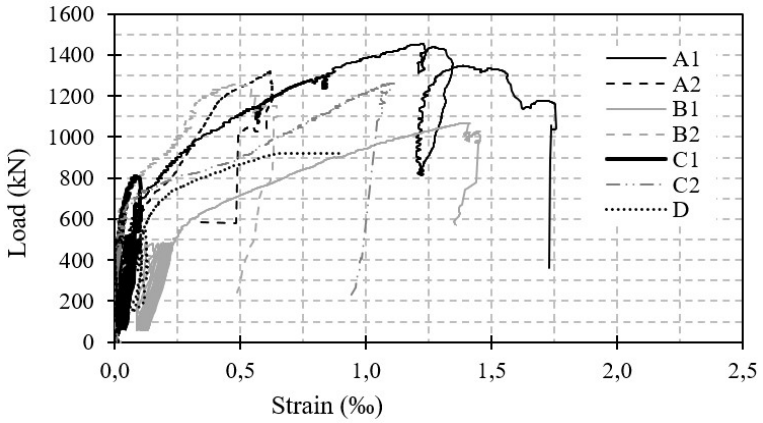

Figure 18. Strain of the slab reinforcement.

Throughout the entire test, the strains observed in the slab bars of all models are elongation ones, due to tensile forces in the reinforcement. For any analyzed loading level, it is evident that the strains in the slab bar of model B1 exceed those of the other models. Models A2 and B2 exhibit similar strain curves, reaching maximum strains slightly above 0.5‰. Analyzing the 800 kN loading for all models, a higher stiffness of the slab reinforcement is observed in models B2 and C1, with strains on the order of 0.1‰ for the analyzed load.

3.5 Concrete Cracking

After the test, the mapping of cracks in the concrete slabs was conducted. Figure 19 illustrates the paths of the cracks that occurred in each model, always considering the most cracked slab in each of them.

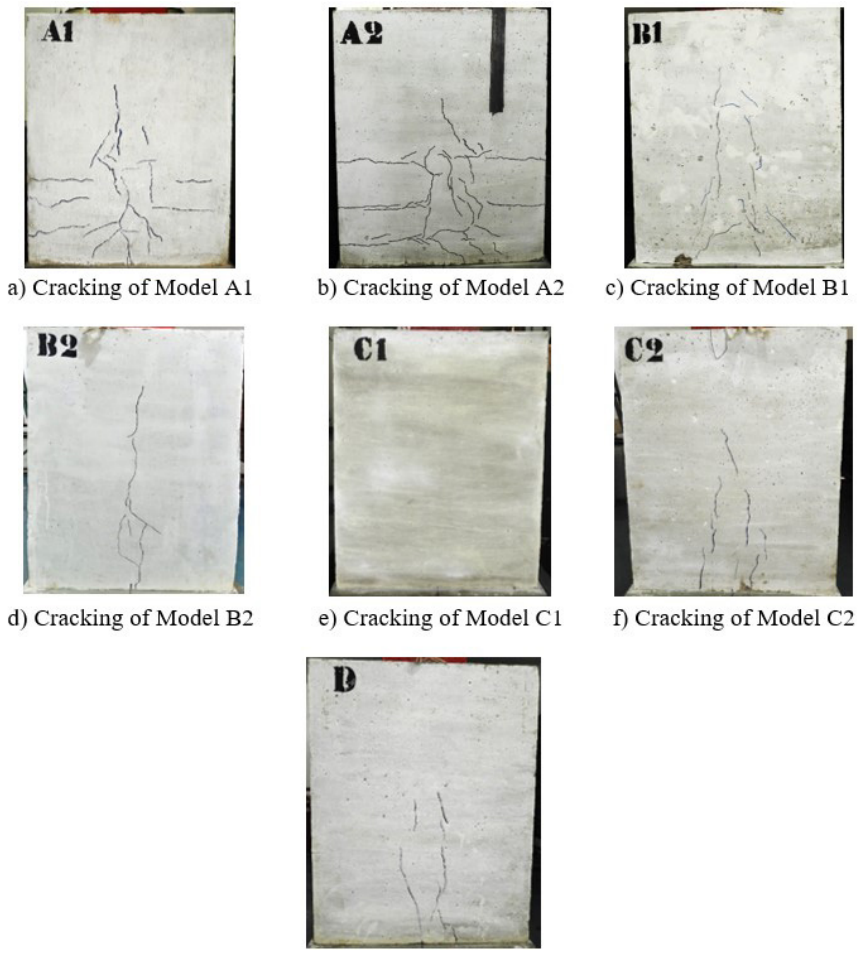

Figure 19. Cracking of models after the test

Models A1 and A2 exhibited the highest levels of cracking at the end of the push-out test. Both models displayed similar crack patterns, featuring vertical (splitting) and diagonal (shear) cracks near the center of the slab, where the connectors were fixed, as well as horizontal cracks (tearing) extending towards the lateral faces, as observed in the figures. The other models did not show significant visible horizontal cracks, only vertical and/or diagonal cracks near the connector attachment areas. Model C1 did not exhibit visible cracks in the concrete slab, possibly due to having a lower reinforcement ratio than the other models, causing the steel to yield before the concrete effectively cracked. Model C2, like Model D, showed some vertical cracks like those in A1, but in fewer numbers.

Except for Model C1, the other analyzed models showed cracking corresponding to splitting to a greater or lesser extent. In Models B1 and B2, the presence of these cracks is more significant than other forms of cracking. In Model B2, where the pair of connectors is inclined in relation to the slab, there is a tendency of a single vertical crack to occur, that starts at the base of the slab and extends up to about 80% of its height, where the last legs of the connectors are located. For Model B1, the vertical splitting cracks occur in two parallel lines approaching the location where the connectors are fixed. Connectors A2 and A1 also exhibit the same behavior, with splitting cracks located near the lines of the upper legs of the shear connectors, as mentioned by Chaves [18]. Table 10 shows the types of cracks observed in the tested models.

Table 10. Types of cracks observed in the model

Model	Type of shear crack		
	Splitting		Tearing
A1	x	x	x
A2	x	x	x
B1		x	
B2		x	
C1			
C2	x		
D	x		

4 CONCLUSIONS

4.1 Failure load

The models have different reinforcement ratio; therefore, it is more coherent to evaluate the load capacity by relating it to the steel area in the shear connection. Connector A1 achieved the best performance compared to the models in this study and those tested by Barbosa [17] and Souza [7], surpassing them by more than 10%. In contrast, models B1 and D showed the worst performances, being about 90% lower than the average.

When compared to connectors tested by Chaves [18] and Veríssimo et al. [19], the connectors in this study exhibit an even more significant gain in load capacity. Analyzing the failure load of the models, gains exceeding 100% were observed when comparing with model A1.

There were no significant indications that the inclination of the connectors positively affects the strength of the models. Model A1 utilizes the transversal area more efficiently compared to A2, which differs only in inclination. On the other hand, Model B1 is less efficient than B2. In the models from Souza [7], variations with inclined positioning of the connectors proved to be less resistant than those positioned at 90° to the profile's flange.

4.2 Relative displacement between the metal profile and the concrete slabs

Models B1 and C1 exhibit the highest relative displacements for low loading levels, immediately after the end of the cyclic phase. Model C1, having a lower reinforcement ratio than the others, fails with just over 800 kN of loading and about 2.70 mm of sliding, ranking as the third most rigid model at the end of the test. Model B1 continues to show higher strains, reaching 10.47 mm of characteristic sliding, making it the most ductile among the analyzed models. Classifying the connectors in ascending order of ductility: D, A1, C1, C2, A2, B2, and B1.

Models with connectors with 10.00 mm of diameter (B1 and B2) exhibit the most ductile behaviors. The influence of the inclination of the connectors on the ductility of the model is not clear. However, Model D is clearly more rigid than the others, reaching 1.09 mm of characteristic sliding. Its high stiffness may be due to the complex geometry of Connector D. In general, the connectors in this study proved to be more rigid than the models tested by Barbosa [17] and Souza [7].

4.3 Transversal separation of the slabs

Among the tested models, Model B1 and Model C1 showed satisfactory behavior regarding uplift according to Eurocode 4 [6], which stipulates that connectors should have a result below 50% of the Up_{80}/δ_{80} ratio. Models B2 and

C2 slightly exceed the limits of the Up_{80}/δ_{80} values. On the other hand, Model D, which performed the worst, exceeded the maximum limit by approximately 4 times.

The models from Souza [7], in general, have higher Up_{80} values, reaching uplift of 2.45 mm in Model TRI. However, they were considered satisfactory since the longitudinal displacement of the profile was also significantly higher. Barbosa [17] reaches maximum uplift values of 1.85 mm for the 12.5 mm rectangle-type connector, and in the Up_{80}/δ_{80} ratio, all connectors show satisfactory performance.

4.4 Strain of shear connectors and slab reinforcement

In general, the strains of the connectors during the cyclic loading phase do not exceed 0.5‰, and in most connectors, more significant strains are observed only at loads exceeding 800 kN. The highest strains were observed in the connectors of models B1 and B2, with 10 mm diameter connectors, and the lowest in models A1 and A2, with 12 mm diameter connectors. C1, which had the lowest reinforcement ratio among the analyzed models, also showed significant strain.

In Model C1, significant strain is noted even in the cyclic phase, reaching 1‰ strain in connector EC1, which could be explained by the reduced reinforcement ratio. Connector EC1 of Model D exhibits much higher strain than the other connectors in the model at all loading phases, reaching strains of more than 2.5‰, while the others do not even reach 1‰ at the end of the test.

ACKNOWLEDGEMENTS

The authors would like to thank CAPES, CNPq, NUMEA, LEC CAMTUC UFPA, Eletrobras/Eletronorte and NDAE for their support in the development of this research.

REFERENCES

[1] J. G. Ollgaard, R. G. Slutter, and J. W. Fisher, "Shear strength of stud connectors in lightweight and normal weight concrete," *AISC Eng. J.*, vol. 8, pp. 55–64, 1971.

[2] G. Queiroz, R. J. Pimenta, and A. Galvão, *Estruturas Mistas, vol. 1*, 2. ed. Rio de Janeiro, RJ, Instituto Aço Brasil.

[3] Associação Brasileira de Normas Técnicas, *Projeto de Estruturas de Aço e de Estruturas Mistas de Aço e Concreto de Edifícios*, NBR 8800, 2008.

[4] American Institute of Steel Construction, *Specification for Structural Steel Buildings*, ANSI/AISC 360-5, 2005.

[5] Canadian Standards Association, *Design of Steel Structures*, S16-09*,* 2009.

[6] European Committee for Standardization, *Eurocode 4 - Design of Composite Steel and Concrete Structures; Part 1.1: General rules and rules for buildings*, 1994-1-1, 2004.

[7] J. P. N. Souza, *Análise experimental de conectores de cisalhamento feitos com aço CA-50 para uso em estruturas mistas de perfis em aço e concreto armado.* Tucuruí, PA: Universidade Federal do Pará, 2019.

[8] Associação Brasileira de Normas Técnicas. *Concreto – Procedimento para moldagem e cura de corpos-de-prova,* NBR 5738, 2003.

[9] Associação Brasileira de Normas Técnicas, *Concreto – Ensaio de Compressão de Corpos-de-prova Cilíndricos*, NBR 5739, 2007.

[10] Associação Brasileira de Normas Técnicas, *Argamassa e Concreto – Determinação de Resistência à Tração por Compressão Diametral de Corpos-de-prova Cilíndricos*, NBR 7222, 2011.

[11] Associação Brasileira de Normas Técnicas, *Concreto – Determinação dos Módulos de Elasticidade e Deformação, NBR 8522*, 2017.

[12] Associação Brasileira de Normas Técnicas, *Determinação da Consistência pelo Abatimento do Tronco de Cone*, NBR NM 67, 1998.

[13] M. V. P. Freitas, "Análise experimental dos limites superiores de resistência à punção de lajes lisas de concreto armado com armaduras de cisalhamento, " Dissertação de mestrado, Núcl. Desenvolv. Amaz. Eng., Univ. Fed. Pará, Tucurí, 2018.

[14] Associação Brasileira de Normas Técnicas. *Materiais Metálicos – Ensaio de Tração. Parte 1: Método de Ensaio à Temperature Ambiente*, NBR ISO 6892-1:2013*,* 2013.

[15] American Society for Testing and Materials. *Métodos Padronizados para Ensaio de Tração De Materiais Metálicos,* ASTM-E8, 2013.

[16] W. D. Callister, *Ciência e engenharia dos materiais: uma introdução*. Tradução Sérgio Murilo Stamile Soares. Rio de Janeiro, LTC, 2002.

[17] W. C. S. Barbosa, "Estudo de conectores de cisalhamento em barras de aço para vigas mistas de aço-concreto," Tese de doutorado, Dept. Eng. Civ. Amb., Univ. Brasília, Brasília, DF, 2016.

[18] I. A. Chaves, "Viga mista de aço e concreto constituída por perfil formado a frio preenchido," Dissertação de mestrado, Esc. Eng. São Carlos, Univ. São Paulo, São Carlos, SP, 2009.

[19] G. S. Veríssimo et al., "Análise experimental de um conector de cisalhamento em chapa de aço endentada para estruturas mistas de aço e concreto," in *Anais XXXII Jorn. Sulam. Eng. Estrut.*, 2006, pp. 410–419.

Author contributions: VCS: conceptualization, data curation, formal analysis, methodology, original draft preparation, writing; ARLF: data curation, formal analysis; AFLN: conceptualization, methodology, formal analysis, supervision.

Editors: Mauro Real, Daniel Carlos Taissum Cardoso.